NASA/TM–20230018517

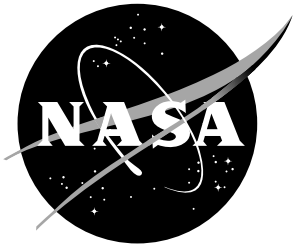

Conceptual Design and Validation of a Bent-Perforation-Path Acoustic Liner

Jordan Kreitzman
Langley Research Center, Hampton, Virginia

January 2024

NASA STI Program Report Series

Since its founding, NASA has been dedicated to the advancement of aeronautics and space science. The NASA scientific and technical information (STI) program plays a key part in helping NASA maintain this important role.

The NASA STI program operates under the auspices of the Agency Chief Information Officer. It collects, organizes, provides for archiving, and disseminates NASA's STI. The NASA STI program provides access to the NTRS Registered and its public interface, the NASA Technical Reports Server, thus providing one of the largest collections of aeronautical and space science STI in the world. Results are published in both non-NASA channels and by NASA in the NASA STI Report Series, which includes the following report types:

- TECHNICAL PUBLICATION. Reports of completed research or a major significant phase of research that present the results of NASA Programs and include extensive data or theoretical analysis. Includes compilations of significant scientific and technical data and information deemed to be of continuing reference value. NASA counterpart of peer-reviewed formal professional papers but has less stringent limitations on manuscript length and extent of graphic presentations.

- TECHNICAL MEMORANDUM. Scientific and technical findings that are preliminary or of specialized interest, e.g., quick release reports, working papers, and bibliographies that contain minimal annotation. Does not contain extensive analysis.

- CONTRACTOR REPORT. Scientific and technical findings by NASA-sponsored contractors and grantees.

- CONFERENCE PUBLICATION. Collected papers from scientific and technical conferences, symposia, seminars, or other meetings sponsored or co-sponsored by NASA.

- SPECIAL PUBLICATION. Scientific, technical, or historical information from NASA programs, projects, and missions, often concerned with subjects having substantial public interest.

- TECHNICAL TRANSLATION. English-language translations of foreign scientific and technical material pertinent to NASA's mission.

Specialized services also include organizing and publishing research results, distributing specialized research announcements and feeds, providing information desk and personal search support, and enabling data exchange services.

For more information about the NASA STI program, see the following:

- Access the NASA STI program home page at http://www.sti.nasa.gov

- Help desk contact information:

https://www.sti.nasa.gov/sti-contact-form/
and select the "General" help request type.

NASA/TM–20230018517

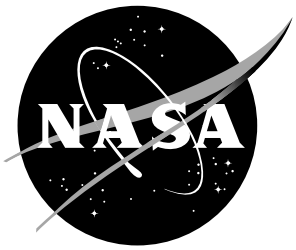

Conceptual Design and Validation of a Bent-Perforation-Path Acoustic Liner

Jordan Kreitzman
Langley Research Center, Hampton, Virginia

National Aeronautics and
Space Administration

Langley Research Center
Hampton, Virginia 23681-2199

January 2024

Acknowledgments

The author would like to acknowledge funding support provided by the Advanced Air Transport Technology Project of the NASA Advanced Air Vehicle Program. The author wishes to acknowledge Mr. Robert Andrews for both developing the sample drawing as well as 3D-printing the sample. The author also wishes to express thanks to Mr. Michael Jones for careful review of this document.

Available from:

NASA STI Program / Mail Stop 050
NASA Langley Research Center
Hampton, VA 23681-2199

Abstract

An acoustic liner concept is developed that increases the effective thickness of perforate sheet holes by bending the perforation paths within the facesheet. This significantly increases both the viscous-loss resistance and mass reactance properties of the acoustic liner, creating low-frequency absorption utilizing a small amount of liner volume. An initial concept is designed, 3D-printed, and tested in a normal-incidence impedance tube to verify the acoustic properties. Comparisons to an impedance model are shown with good agreement to test data, although further work needs to be done to more accurately capture the losses associated with bends within the hole. Follow-on concepts are also discussed that attempt to address the current shortcomings of the initial design.

Nomenclature

Symbols	**Description**
α	normal-incidence absorption coefficient
b	chamber depth
c, ρ	air speed of sound and density
C_D, C_P, C_V	discharge coefficient and specific heat at constant pressure and volume
d, d_c	perforate sheet hole and chamber diameter
$\gamma, \kappa, \mu, \sigma^2$	air specific heat ratio, thermal conductivity, dynamic viscosity, and Prandtl number
Γ, n	propagation constant and value used during calculation procedure
j	imaginary number, $\sqrt{-1}$
$J_m()$	Bessel function of the first kind of order m
k, s, ω, T	free-space wavenumber, shear wavenumber, angular frequency, and time
Ω	ratio of the acoustically active surface area to the total surface area of the liner
p_B	iterated value for acoustic pressure at the backplate, normalized by ρc^2
p_i, p_{iH}	acoustic pressure at i^{th} liner position and inside perforate hole, normalized by ρc^2
ϕ, t	perforate sheet open area ratio (OAR) and thickness
T_{ij}	transmission coefficient
θ, θ_{nl}	liner resistance and perforate sheet nonlinear resistance, normalized by ρc
u_i, u_{iH}	particle velocity at i^{th} liner position and inside perforate hole, normalized by c
χ, χ_e	liner reactance and perforate sheet radiation reactance, normalized by ρc
ζ, ζ_c	liner surface impedance and element characteristic impedance, normalized by ρc

1 Introduction

Future aircraft continue to trend toward higher bypass ratio engines and shorter length nacelles for increased fuel efficiency. This negatively impacts the effectiveness of current acoustic liner treatments on fan noise, not only because of reduced treatment area but also because dominant fan noise is transitioning to lower frequencies. Therefore, it is important to investigate ways of improving acoustic liner absorption at lower frequencies, especially solutions that do not require additional space or weight.

A single-degree-of-freedom (SDOF) acoustic liner shown in Fig. 1 is composed of a perforate facesheet over honeycomb with a rigid backing. The acoustic characteristics of a liner can be defined

by its surface impedance, which is the ratio of the acoustic pressure to the acoustic particle velocity normal to the liner surface. This can be seen as Eq. (1) below, where the terms are normalized by the characteristic impedance of the environment air.

$$\zeta = \frac{p}{\rho c u_n} = \theta + j\chi \tag{1}$$

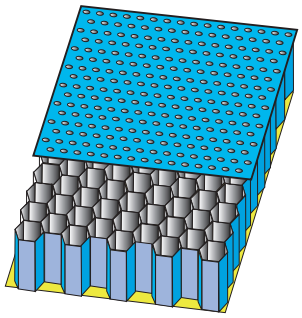

Figure 1: Single-degree-of-freedom (SDOF) liner with a standard perforate facesheet [Source: NASA].

The impedance contains both real (resistive) and imaginary (reactive) components, with contributions from both the facesheet and honeycomb. One way to improve the low-frequency absorption of the acoustic liner is by increasing the facesheet reactance. This is typically done by altering the thickness, hole diameter, or open area ratio (OAR). Weight concerns due to thick facesheets limit options in that regard. Additionally, dropping the OAR or increasing the hole diameter can lower the target absorption frequencies. However, a large hole diameter is not desirable due to resistance degradation and increased drag [1], while lowering the OAR increases sensitivity of liner performance to the sound and hydrodynamic environment, which is often an undesirable trait for an aircraft liner design.

Perforate sheet resistance tends to be very sensitive to the sound pressure level (SPL) of the incident source to which it is exposed. This is due to nonlinear effects of the acoustic particle velocity, where there are turbulent mixing losses associated with the acoustic waves exiting the holes. This can present a challenge to acoustic liner design for an engine nacelle that will experience a wide variety of noise intensities during flight. It is often preferred to have an acoustic liner be dominated by linear viscous losses instead, since these losses are essentially independent of SPL. However, this tends to be very difficult in practice for a perforate facesheet, unless the facesheet has very small holes (i.e., microperforate dimensions) or is very thick. Additionally, the acoustic liner OAR needs to be relatively high in order to mitigate the SPL-driven resistance, and this further reduces the impact of the viscous-loss resistance.

A bent-perforation-path acoustic liner attempts to (1) provide a reactance increase to improve lower-frequency absorption and (2) reduce sensitivity to the incident sound pressure level while maintaining its target resistance requirements. To accomplish this, the effective thickness of the facesheet holes is increased by bending the perforation paths within the facesheet. A simple example of the proposed change can be seen in Fig. 2. The actual facesheet thickness is not impacted, but rather the perforation holes bend and extend within the plane of the facesheet, thereby extending

the propagation paths of the holes. In doing this, facesheet reactance and viscous-loss resistance are significantly increased.

Figure 2: Proposed design change for a facesheet perforate hole. Propagation paths illustrated with an arrow.

The intent of the current study is to design, print, and test an acoustic liner concept that includes the bent-perforation-path facesheet. The desire is to validate the capability of the concept and not derive an optimized design at this stage. In the following sections, the conceptual design that was printed will be shown in detail. The model used to help characterize the impedance of the design will then be shown. This will be followed by a description of the impedance tube used during the test as well as test conditions considered. Finally, a discussion of the results with comparisons to the model will be provided, along with descriptions of follow-on concepts.

2 Conceptual design

The conceptual design for the bent-perforation-path acoustic liner shown in Fig. 3 was 3D-printed via stereolithography (SLA). Please note that the images include transparency of the facesheet and partitions to improve the view of the bent-perforation paths. The geometric parameters of the acoustic liner are shown in Table 1. The acoustic liner was printed as one integrated piece (facesheet and chambers together) to improve structural rigidity. A chamber depth of 1.5" was selected to back the facesheet, which is representative of space typically available within an engine nacelle. As mentioned in the previous section, this is not an optimized design but is simply an attempt to demonstrate the concept. The "Facesheet effective hole diameter" referenced in Table 1 refers to the diameter of a circular perforation of equivalent cross-sectional area to the square perforation that was used. Additionally, the "Facesheet perforation midline length" is referring to the midline length through the bent path of the perforation. It should be noted that there was no quality assurance performed on the sample (i.e., no measurements were taken to verify geometric parameters were printed properly) other than a visual inspection of the sample. Due to the unique nature of the sample, certain geometric parameters cannot be measured easily.

The perforation paths are maximized by starting the holes near one edge of the chamber cross-section and having them exit near the other edge. To do this, the perforation paths go down a small distance into the facesheet, perform a 90-degree bend, go across most of the width of the chamber cross-section, and then perform another 90-degree bend and exit to the lower side of the facesheet. Figure 3d shows a diagram of a single chamber, where the white squares indicate the openings at the top of the facesheet, and the red squares denote where the holes exit to the air chamber backing the facesheet. The section cut also shown in this diagram displays the perforation path within the facesheet. Square perforation shapes were chosen for this conceptual design to minimize the complexity of the perforation bends. Some preliminary impedance tube testing conducted before

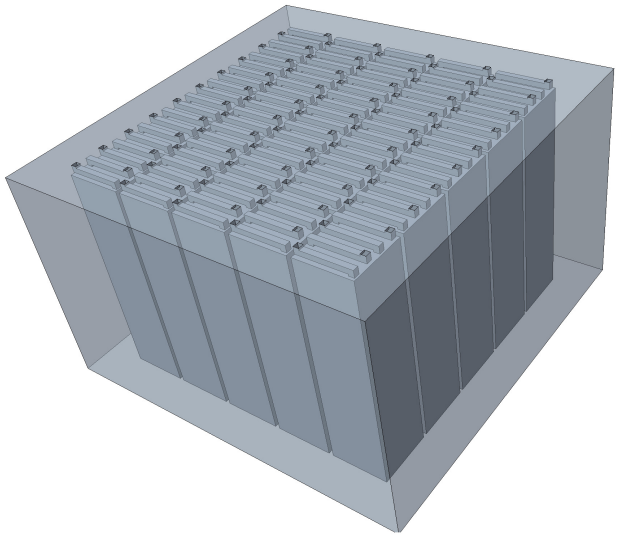

(a) Isometric view

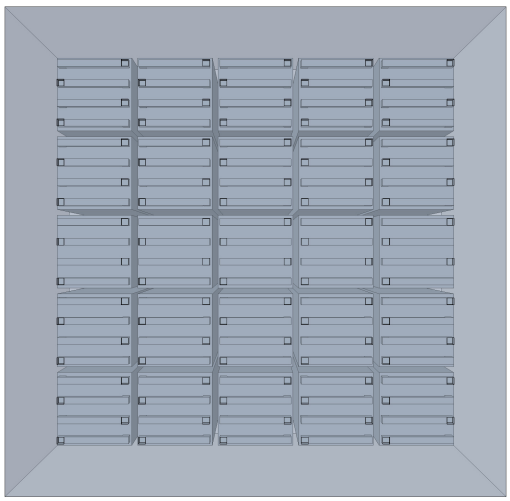

(b) Top view

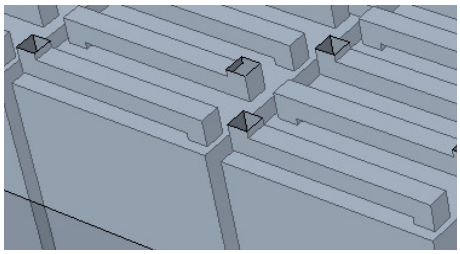

(c) Zoomed-in view of the facesheet holes

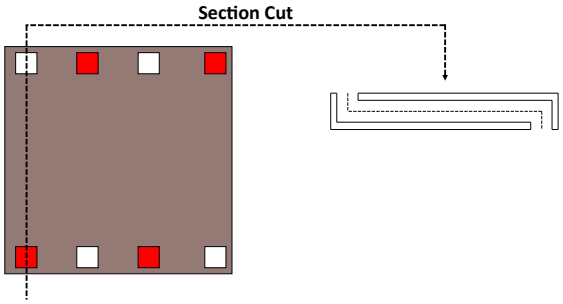

(d) Single-chamber diagram

Figure 3: Conceptual design of the bent-perforation-path acoustic liner.

this study confirmed that the performance of a square perforation was nearly identical to a circular perforation of the same cross-sectional area.

It is important to note that the acoustic liner OAR is very low. Future studies will explore ways to help raise the OAR of the bent-perforation-path acoustic liner, as a low OAR increases both SPL-driven resistance and grazing-flow resistance. A concept for raising the OAR will be shown later in the report. The overall goal of the preliminary conceptual design is to increase the effective thickness of the facesheet perforation holes, thereby increasing the mass reactance and viscous-loss resistance of the liner. It is seen in Table 1 that a facesheet thickness of 0.06" is utilized (reasonable

Table 1: Geometric parameters of the bent-perforation-path acoustic liner.

Geometric parameters	Values
Array layout	5x5
Chamber size	0.375"x0.375"
Partition thickness	0.0300"
Chamber depth (b)	1.50"
Facesheet open area ratio (OAR) (ϕ)	0.0357
Facesheet thickness (t)	0.0600"
Facesheet perforation shape	Square
Facesheet effective hole diameter (d)	0.0400"
Facesheet perforation midline length	0.380"

for modern engine nacelles) but the perforation midline length has been increased dramatically to 0.38".

3 Impedance prediction model

The impedance prediction tool used for this study is based on theory from the NASA Zwikker and Kosten Transmission Line (ZKTL) impedance prediction code [2–4], where the acoustic pressures and velocities are calculated by stepping through the acoustic liner, from the backplate to the liner surface. Figure 4 shows the computational layers for a single acoustic liner channel, where the thickness of the perforate sheet has been exaggerated for the clarity of the drawing. It should be noted that the acoustic liner channel of interest in this study is a perforate sheet backed by an air chamber, where it is assumed in the model that the bent-perforation paths of the holes are actually straight. The midline length (or effective thickness) of the holes is then used as the facesheet thickness in the model. Recent research has used the work demonstrated in Cummings [5] to modify the midline length to account for bends and sharp corners of bent chambers, thereby better predicting the impedance [6, 7]. This was explored as an option in this study, but ultimately it was found that using the midline length without any corrections provided the best impedance prediction. It should also be noted that for both the predictions and test data impedances shown in this paper, the $e^{j\omega T}$ time convention is used.

The current code implements an iterative method at the backplate of the liner to adjust the acoustic pressure until the surface pressure matches the target SPL. Therefore, this method attempts to account for the acoustic particle velocity effects at the facesheet. The backplate is assumed rigid with the acoustic pressure and velocity starting values given by Eq. (2) below, where these values are normalized by ρc^2 and c, respectively.

$$\begin{pmatrix} p_0 \\ u_0 \end{pmatrix} = \begin{pmatrix} p_B \\ 0 \end{pmatrix} \tag{2}$$

The value p_B is the current iterated guess for the backplate acoustic pressure. This value will update after every iteration utilizing a simple bisection method. For the air chamber, the acoustic pressure and velocity at the top of the chamber can be calculated via transmission coefficients using the acoustic pressure and velocity at the bottom of the chamber, see Eqs. (3) and (4) below.

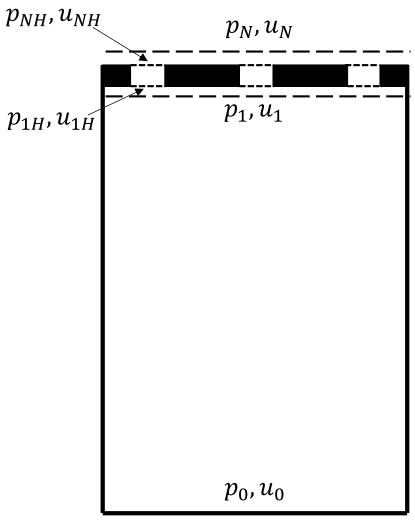

Figure 4: Example of computational layers in the acoustic liner impedance prediction tool.

$$\begin{pmatrix} p_{i+1} \\ u_{i+1} \end{pmatrix} = \begin{pmatrix} T_{11} & T_{12} \\ T_{21} & T_{22} \end{pmatrix} \begin{pmatrix} p_i \\ u_i \end{pmatrix} \tag{3}$$

$$T_{11} = T_{22} = \cosh(k\Gamma b); T_{12} = \zeta_c \sinh(k\Gamma b); T_{21} = \zeta_c^{-1} \sinh(k\Gamma b) \tag{4}$$

To calculate the transmission coefficients, one must first solve for the propagation constant, Γ, and characteristic impedance, ζ_c. This is done by solving for the shear wavenumber, s, as well as the Prandtl number, σ^2, and the specific heat ratio, γ, all shown in Eq. (5).

$$s = \frac{d_c}{2}\sqrt{\frac{\rho\omega}{\mu}}; \sigma^2 = \mu\frac{C_P}{\kappa}; \gamma = \frac{C_P}{C_V} \tag{5}$$

The propagation constant is then calculated as Eq. (6) below, where the n value in the propagation constant formulation is also shown.

$$\Gamma = \sqrt{\frac{J_0(j^{3/2}s)}{J_2(j^{3/2}s)}}\sqrt{\frac{\gamma}{n}}; n = \left[1 + \frac{\gamma-1}{\gamma}\frac{J_2(j^{3/2}\sigma s)}{J_0(j^{3/2}\sigma s)}\right]^{-1} \tag{6}$$

Once the propagation constant is calculated, the characteristic impedance can be calculated via Eq. (7).

$$\zeta_c = \frac{-j}{\Gamma}\frac{J_0(j^{3/2}s)}{J_2(j^{3/2}s)} \tag{7}$$

This is the basic structure for solving the acoustic pressures and velocities within the air chamber of the liner. A similar model can also be used to calculate the transfer impedance of the top layer facesheet. The wave propagation model shown in Jones et al. [8], recently assessed for accuracy in Jones et al. [9], is used with some added modifications that were first reported in Kreitzman et al. [10]. It is assumed that as one goes from an air chamber to a single perforate hole, continuity

of acoustic pressure is maintained while the acoustic particle velocity increases due to conservation of mass. Equation (8) below shows the assumptions being made.

$$p_{iH} = p_i; u_{iH} = \frac{u_i}{\phi} \tag{8}$$

Once the acoustic pressure and velocity are defined at the entrance of a given perforate hole, Eqs. (3)–(7) can be used again to calculate the acoustic pressure and velocity at the other side of the hole, noting of course that instead of the chamber diameter, d_c, and chamber depth, b, being used, the perforate sheet hole diameter, d, and sheet thickness, t, are used. Once the acoustic pressure and velocity are defined at the other end of the perforate hole, similar logic to that shown in Eq. (8) can be applied for the acoustic pressures and velocities just above the holes. Equation (9) below shows this.

$$p_{i+1} = p_{(i+1)H}; u_{i+1} = u_{(i+1)H}\phi \tag{9}$$

There are additional assumptions that can be made to further modify Eq. (9). For one, this method for the impedance prediction does not capture the nonlinear resistance of a perforate caused by the turbulent mixing loss of the acoustic waves exiting the holes. Equation (10) can be used to account for this [11].

$$\theta_{nl} = \frac{(1-\phi^2)}{2\phi^2 C_D^2}|u_{i+1}| \tag{10}$$

Additionally, this model only properly accounts for acoustic behavior inside the holes and neglects the radiation impedance effects, typically applied using a mass-end-correction term in the reactance. This term is given in Eq. (11) below for a normal incidence environment [12]. Note that this equation is formulated for a uniformly-distributed perforate facesheet, and as shown in Fig. 3b, the conceptual design does not have a uniform perforate hole layout. Work is ongoing to more appropriately model radiation impedances for nonuniformly-distributed perforate facesheets [13].

$$\chi_e = 0.85kd\frac{1-1.25\sqrt{\phi}}{\phi} \tag{11}$$

Equation (9) for the acoustic pressure can be modified with Eqns. (10) and (11) to represent an additional acoustic pressure change associated with the nonlinear resistance and radiation reactance, shown below as Eq. (12). Note that the perforate sheet is treated as a lumped element (i.e., no change of particle velocity across the sheet) for these added terms.

$$p_{i+1} = p_{(i+1)H} + (\theta_{nl} + j\chi_e)u_{i+1} \tag{12}$$

The normalized surface impedance of an acoustic liner is then defined in Eq. (13), where the impedance of a single acoustic liner channel is the ratio of the normalized acoustic pressure to acoustic particle velocity at the surface of the liner. To account for partitions between these channels, this definition is then divided by the ratio of the acoustically active surface area to the total surface area of the liner exposed to the incident source, Ω. This definition is only valid for acoustic liners where the impedance does not change between channels, which for the purposes of this paper is a valid approximation.

$$\zeta = \frac{1}{\Omega}\frac{p_n}{u_n} \tag{13}$$

In addition to the surface impedance, normal incidence absorption coefficients (α) are calculated using Eq. (14) below utilizing the resistance (θ) and reactance (χ) terms of the calculated surface impedance (ζ).

$$\alpha = \frac{4\theta}{(1+\theta)^2 + \chi^2} \tag{14}$$

4 Normal Incidence Tube (NIT) test rig

The test is conducted in a normal incidence impedance tube, specifically the NASA Normal Incidence Tube (NIT). The NASA NIT is a 2" x 2" waveguide of approximately 36" in length. It uses six 120 W compression acoustic drivers to generate a sound field that impinges on the acoustic liner surface. There are 3 flush-mounted microphones associated with the rig. One is a reference microphone 0.25" away from the sample surface and is used to help achieve the appropriate total SPL (incident plus reflected) for the test. Two other microphones are then placed 2.50" and 3.75" from the liner surface and are mounted in a rotating plug so that their positions can be interchanged. This allows errors associated with the amplitudes and phases due to mismatched microphone calibrations to be eliminated during the two-microphone method process [14]. The NIT allows for 4 different source types: stepped-sine, swept-sine, multitone, and broadband. For this study, swept-sine is used, which is a controlled amplitude swept-sine source that can maintain ±0.5 dB amplitude accuracy with approximately 5 Hz analysis resolution from 400–3,000 Hz [15]. A drawing of the NIT is shown in Fig. 5. For this particular test, the sample was tested at 120, 130, and 140 dB.

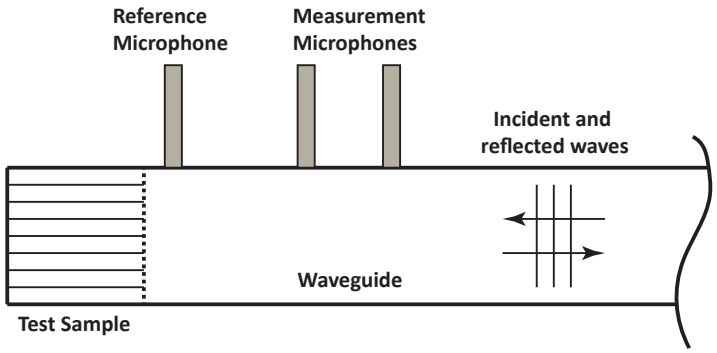

Figure 5: Normal Incidence Tube (NIT) test rig [Source: NASA].

5 Analysis of results

Figures 6 and 7 show the test data and predictions of the bent-perforation-path acoustic liner at 120, 130, and 140 dB. It is shown that the prediction model aligns quite well with the test data absorption, reactance, and acoustic liner resonant frequency, where resonance is defined where the reactance curve crosses zero with a positive slope. There is only one prediction line shown for the reactance, as the model predicts the same values across all SPLs. The test data show a shift in the resonance to slightly higher frequencies as the SPL is increased. This is well-known behavior as the

particle velocity effect lowers the mass-end-correction term of the radiation impedance [11]. This effect is not currently included in the impedance model. The model also appears to under-predict the resistance away from resonance and strong particle velocity effects. It is theorized that since the model is assuming a straight hole, it is not capturing additional losses associated with the tight bends within the perforation pattern. This will need to be studied further if these types of acoustic facesheets are to be modeled more accurately in the future.

It should also be noted that the discharge coefficient, C_D, was used as a tuning parameter for the resistance at the 130 dB case. C_D values in the model typically range from 0.75–0.90 for standard perforate facesheets. Due to the uniqueness of the bent-perforation-path facesheet, it was decided to adjust C_D to match the resistance data near resonance at 130 dB. It should be noted that this approach is really only tuning the nonlinear resistance due to the SPL, as the particle velocity effects are strongest at resonance. In doing this, a value of 0.45 was used for the C_D in the model, which is much lower than typically used values. However, due to the unique propagation path of the acoustic waves through the holes, this may be physically realistic. More investigation on this matter should be explored further. The value of 0.45 was then used to predict data at both 120 and 140 dB, and it is seen that the resistances near resonance are well predicted.

One can see in Fig. 6 that the peak absorption frequency of the liner sample hovers around 500 Hz for all three SPL values. This is a low frequency considering the chamber depth behind the facesheet is only 1.5". The large effective thicknesses of the perforation holes greatly increase the mass reactance of the facesheet. For comparison, the model was used to predict the impedance of an acoustic liner with the same geometric parameters as the conceptual design, only with the holes straightened out like a typical facesheet. This drops the facesheet thickness used in the model down to 0.06". In this case, the peak absorption frequency is almost 1,000 Hz, indicating that the bent-perforation paths of the conceptual design lower the resonance by 500 Hz.

As mentioned earlier, the conceptual design shown here has a particularly low OAR, and Fig. 7 clearly shows that the resistance is strongly affected by the SPL. The intent of the conceptual design was to increase both the mass reactance and viscous-loss resistance of the facesheet. One can see in Fig. 7 that both of these have been achieved, as even at 120 dB where particle velocity effects are lower, the resistance is still of a sufficient magnitude. The next step in the progress of this concept is to increase the OAR to mitigate the SPL-driven resistance. A preliminary concept for this is shown in the next section.

6 Next Steps

It was shown in this report that the low OAR corresponds to high sensitivity of resistance to the incident SPL. This sensitivity is typically undesirable for aircraft liner design, therefore raising the OAR of this concept is critical. One way of doing this is through the use of two layers of perforation bends. This would allow perforations to bend underneath one another, and therefore more holes could be placed on the surface. A potential perforation layout of this concept is shown in Fig. 8. For this example, if the facesheet thickness was extended to 0.11", up to 10 holes could be placed on the surface. This would raise the OAR from 0.0357 to 0.0893, reducing sensitivity to acoustic particle velocity and therefore SPL. It should be noted that this comes at the expense of more liner volume and potentially added weight, although adding more perforation paths through the facesheet may minimize any weight gain.

Another negative drawback of the concept is its narrow high-absorption frequency range. Al-

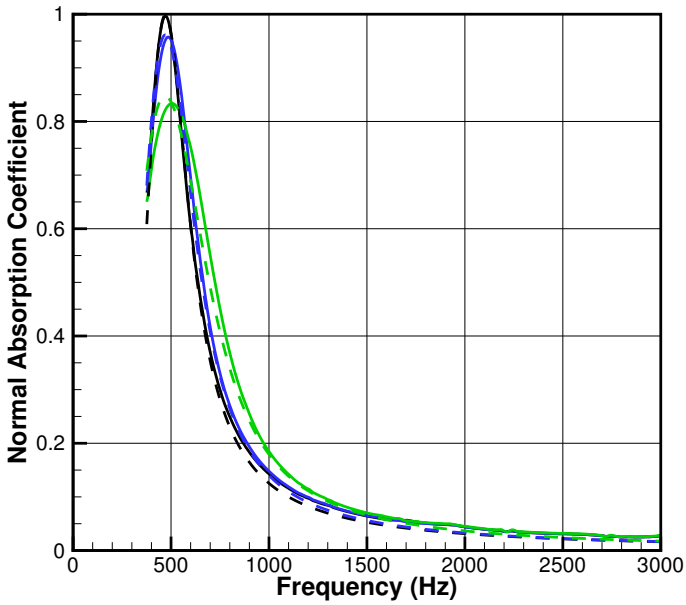

Figure 6: Normal incidence absorption coefficient at 120 dB (black line), 130 dB (blue line), and 140 dB (green line). Solid lines are test data; dashed lines are predictions. Good agreement between predictions and test data is seen across the full frequency and sound pressure level (SPL) range.

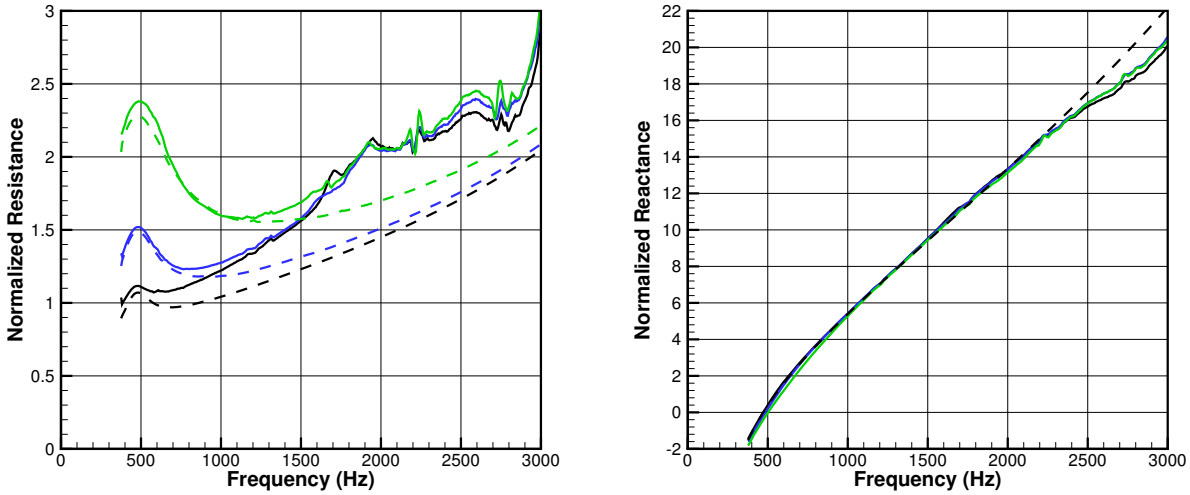

(a) Normalized resistance

(b) Normalized reactance

Figure 7: Normalized impedance vs. frequency (Hz) at 120 dB (black line), 130 dB (blue line), and 140 dB (green line). Solid lines are test data; dashed lines are predictions. Good agreement between predictions and test data reactance is seen across the full frequency range, but more work is needed to accurately predict the resistance away from resonance.

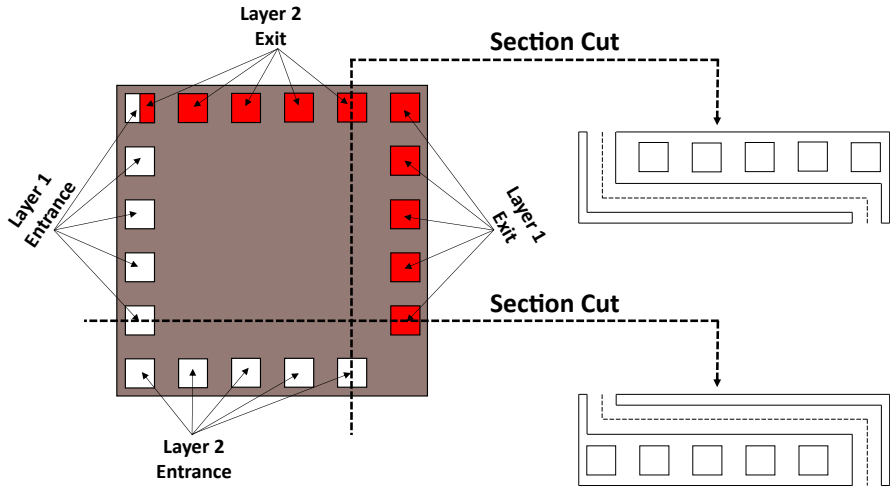

Figure 8: Preliminary concept for a two-layer, bent-perforation-path acoustic liner. Diagram shown is for a single chamber.

though the intent of the conceptual design was to target a single low frequency, often an acoustic liner is needed to provide high absorption over a wide range of frequencies. A drawback to adding high amounts of mass reactance to a liner system is that the acoustic liner's high-absorption characteristics only exist over a small frequency range. One potential way to mitigate this issue is through the use of variable-length perforation paths within the chambers. Similar to work performed on variable-depth acoustic liners [4, 6, 8], variable-length perforation paths would, in theory, broaden the absorption characteristics of the acoustic liner. Both one and two-layer bend concepts could employ this, but it should be noted that variable-length perforations for the two-layer bend concept would be restricted to the second lower layer.

Another potential use of the bent-perforation-path facesheet is coupling it with a larger cross-section chamber. This would enable even longer bent-perforation paths, further lowering the resonant frequency of the liner system. Recent research indicates that large chambers can maintain local impedance behavior up to a 2" x 2" cross-section in a grazing incidence environment for frequencies that are of interest in this paper [16, 17]. One would need to be careful with this design possibility though, as the viscous-loss resistance may get excessively high for long bent-perforation paths. Additionally, it was noted in Kreitzman et al. [13] that vibration issues can exist for facesheets with large cross-section chambers backing them. Despite these potential issues, the possibility of the concept should be explored further to assess the design space. Future work should also include varying the chamber depth behind the bent-perforation-path facesheet to provide more insight into impedance characteristics and further validate the impedance prediction model.

7 Summary

Low-frequency absorption characteristics are needed for future acoustic liners on engine nacelles, where space and weight are extremely limited. A space-efficient approach to lower-frequency absorption is the bent-perforation-path acoustic liner, which bends the propagation paths of the holes in the facesheet to increase the effective hole thickness. This adds significant mass reactance and viscous-loss resistance to the acoustic liner. A bent-perforation-path acoustic liner was designed, 3D-printed, and tested in a normal incidence impedance tube. It was found that for a 1.5" chamber depth and 0.06" facesheet thickness, the bent-perforation-path acoustic liner lowered the resonant frequency down to ∼500 Hz. Next steps are in place to look at additional concepts that (1) raise the OAR to lower SPL sensitivity and (2) vary the perforation-path lengths within the chamber to broaden the high-absorption frequency range. Larger chamber cross-sections will also be explored to assess longer perforation paths.

References

1. B. Howerton and M. Jones, "Acoustic Liner Drag: A Parametric Study of Conventional Configurations," *AIAA 2015-2230*, 2015.

2. C. Zwikker and C. Kosten, *Sound Absorbing Materials*. Elsevier, Amsterdam, 1949.

3. H. Tijdeman, "On the propagation of sound waves in cylindrical tubes," *Journal of Sound and Vibration*, vol. 39, no. 1, pp. 1–33, March 1975.

4. T. Parrott and M. Jones, "Parallel Element Liner Impedances for Improved Absorption of Broadband Sound in Ducts," *Noise Control Engineering Journal*, vol. 43, no. 6, pp. 183–195, 1995.

5. A. Cummings, "Sound Transmission in Curved Duct Bends," *Journal of Sound and Vibration*, vol. 35, no. 4, pp. 451–477, 1974.

6. M. Jones, D. Nark, and N. Schiller, "Evaluation of Variable-Depth Liners with Slotted Cores," *AIAA 2022-2823*, 2022.

7. D. Nark and M. Jones, "A Fundamental Study of Bifurcation Acoustic Treatment Effects on Aft-Fan Engine Noise," *AIAA 2023-3345*, 2023.

8. M. Jones, B. Howerton, and E. Ayle, "Evaluation of Parallel-Element, Variable-Impedance, Broadband Acoustic Liner Concepts," *AIAA 2012-2194*, 2012.

9. M. Jones and D. Nark, "Comparisons of Impedance Prediction Models for Perforate-over-Honeycomb Liners," *AIAA 2023-3637*, 2023.

10. J. Kreitzman and M. Jones, "Toward Fully 3D-Printed Two Degree of Freedom Acoustic Liners," *AIAA 2024-2801*, 2024.

11. U. Ingard and H. Ising, "Acoustic Nonlinearity of an Orifice," *The Journal of the Acoustical Society of America*, vol. 42, no. 1, pp. 6–17, 1967.

12. U. Ingard, "On the Theory and Design of Acoustic Resonators," *The Journal of the Acoustical Society of America*, vol. 25, no. 6, pp. 1037–1061, 1953.

13. J. Kreitzman and M. Jones, "Investigation of the impedance characteristics of perforate sheet hole clustering over an array of uniform depth chambers," *AIAA 2024-2800*, 2024.

14. J. Chung and D. Blaser, "Transfer function method of measuring in-duct acoustic properties: I. theory," *Journal of the Acoustical Society of America*, vol. 68, pp. 907–921, 1980.

15. M. Jones, W. Watson, D. Nark, B. Howerton, and M. Brown, "A Review of Acoustic Liner Experimental Characterization at NASA Langley," *NASA TP-2020-220583*, 2020.

16. M. Brown and M. Jones, "Effects of Cavity Diameter on Acoustic Impedance of Perforate-Over-Honeycomb Liners," *AIAA 2017-4189*, 2017.

17. M. Brown, C. Dodge, J. Kreitzman, and M. Jones, "Assessment of Acoustic Behavior for Perforate-Over-Large-Cell Liners," *AIAA 2023-3501*, 2023.

REPORT DOCUMENTATION PAGE	Form Approved OMB No. 0704–0188

1. REPORT DATE *(DD-MM-YYYY)*	2. REPORT TYPE	3. DATES COVERED *(From - To)*
01-12-2023	Technical Memorandum	

4. TITLE AND SUBTITLE
Conceptual Design and Validation of a Bent-Perforation-Path Acoustic Liner

5a. CONTRACT NUMBER

5b. GRANT NUMBER

5c. PROGRAM ELEMENT NUMBER

6. AUTHOR(S)
Jordan Kreitzman

5d. PROJECT NUMBER

5e. TASK NUMBER

5f. WORK UNIT NUMBER

7. PERFORMING ORGANIZATION NAME(S) AND ADDRESS(ES)
NASA Langley Research Center
Hampton, Virginia 23681-2199

8. PERFORMING ORGANIZATION REPORT NUMBER

9. SPONSORING/MONITORING AGENCY NAME(S) AND ADDRESS(ES)
National Aeronautics and Space Administration
Washington, DC 20546-0001

10. SPONSOR/MONITOR'S ACRONYM(S)
NASA

11. SPONSOR/MONITOR'S REPORT NUMBER(S)
NASA/TM–20230018517

12. DISTRIBUTION/AVAILABILITY STATEMENT
Unclassified-Unlimited
Subject Category
Availability: NASA STI Program (757) 864-9658

13. SUPPLEMENTARY NOTES
An electronic version can be found at http://ntrs.nasa.gov.

14. ABSTRACT
An acoustic liner concept is developed that increases the effective thickness of perforate sheet holes by bending the perforation paths within the facesheet. This significantly increases both the viscous-loss resistance and mass reactance properties of the acoustic liner, creating low-frequency absorption utilizing a small amount of liner volume. An initial concept is designed, 3D-printed, and tested in a normal-incidence impedance tube to verify the acoustic properties. Comparisons to an impedance model are shown with good agreement to test data, although further work needs to be done to more accurately capture the losses associated with bends within the hole. Follow-on concepts are also discussed that attempt to address the current shortcomings of the initial design.

15. SUBJECT TERMS
acoustic, liner, perforate, impedance

16. SECURITY CLASSIFICATION OF:			17. LIMITATION OF ABSTRACT	18. NUMBER OF PAGES	19a. NAME OF RESPONSIBLE PERSON
a. REPORT	b. ABSTRACT	c. THIS PAGE			STI Information Desk (help@sti.nasa.gov)
U	U	U	UU	20	19b. TELEPHONE NUMBER *(Include area code)* (757) 864-9658